Title	Enhancement of plastic anisotropy and drastic increase in yield stress of Mg-Li single crystals by Al-addition followed by quenching
Author(s)	Hagihara, Koji; Mori, Keitaro; Nakano, Takayoshi
Citation	Scripta Materialia. 172 p.93-p.97
Issue Date	2019-11-01
oaire:version	VoR
URL	https://hdl.handle.net/11094/89813
rights	This article is licensed under a Creative Commons Attribution 4.0 International License.
Note	

Enhancement of plastic anisotropy and drastic increase in yield stress of Mg-Li single crystals by Al-addition followed by quenching

Koji Hagihara [a,*], Keitaro Mori [a], Takayoshi Nakano [b]

[a] Department of Adaptive Machine Systems, Graduate School of Engineering, Osaka University, 2-1 Yamadaoka, Suita, Osaka 565-0871, Japan
[b] Division of Materials and Manufacturing Science, Graduate School of Engineering, Osaka University, 2-1 Yamadaoka, Suita, Osaka 565-0871, Japan

A B S T R A C T

Strong orientation dependence of yield stress was found in a body-centered cubic (bcc)-structured Mg-Li alloy single crystal by adding 5 at.% of Al combined with rapid quenching, which was negligible in Mg-Li binary single crystals.

Furthermore, the addition of 5 at.% of Al combined with rapid quenching caused an extreme increase in yield stress up to ~470 MPa; this compares to ~50 MPa in a Mg-Li binary crystal. Increased valence-electron to atom ratio and development of chemical modulation in the alloy by Al-addition are probable causes of the enhancement of plastic anisotropy and the drastic increase in yield stress, respectively.

© 2019 Published by Elsevier Ltd on behalf of Acta Materialia Inc.

Because of the growing interest in environmental issues, Mg alloys as lightweight structural materials have generated increasing interest [1]. Moreover, Mg alloys are noble "biodegradable materials" that do not require secondary surgery for removal after implantation in the body [2]. However, a serious problem with Mg alloys is their low workability derived from their hexagonal close-packed (hcp) structure. To overcome this, the structural change to bcc-structure by adding more than ~30 at.% Li is extremely promising [3]. Practical uses of Mg-Li alloys in personal computer frames etc. are being implemented; however, further improvements in strength and corrosion resistance are needed. The studies on how to control these material properties are still not sufficient. Specifically, there have been few reports that clarify the dependence of the properties on the crystal orientation [4].

In our laboratories, we have been developing "single crystalline implants" using bcc-Ti alloys [5,6]. We have demonstrated that the use of single crystals with controlled crystal orientation is an excellent way to manage the mechanical properties. The Young's modulus of a polycrystalline bcc-Ti alloy (~65 GPa) can be reduced to ~35 GPa in a single crystal aligned along $\langle 100 \rangle$ [7]. This value is close to that of human cortical bone: ~10–30 GPa [8]. According to the ab initio calculation, the Young's modulus of Mg-30 at.%Li polycrystalline alloy is expected to be ~46 GPa [9], which is much smaller than that of bcc-Ti alloys. Thus, crystal orientation control in the Mg-Li alloys has intriguing possibilities for fine-tuning the Young's modulus of biodegradable implants to that of human bone. Furthermore, we have confirmed that the degradation

behavior of the hcp-Mg single crystal can be controlled over a wide range by crystal orientation control [10]. Thus, the study of bcc Mg-Li single crystals is essential not only to broaden their conventional practical applications, but also for the development of a noble "biodegradable single-crystalline implant".

We have examined the orientation dependence of deformation behavior of bcc Mg-Li-Al single crystals in this study. Most of the recently developed bcc Mg-Li alloys contain Al to improve the corrosion properties [11], but the influence of the added Al on the mechanical properties has not yet been sufficiently clarified [12]. On the strength, Tang et al. recently reported the significant increase in yield stress of Mg-Li polycrystalline alloy by Al-addition [13]. Thus, we focused on Mg-Li-Al single crystals. As a result, the enhancement of plastic anisotropy, accompanied by a drastic increase in yield stress up to ~470 MPa was found in the single crystal by the addition of 5 at.% of Al. The origins of these phenomena are discussed.

We focused on two alloys with atomic compositions of (Mg-36.6Li)$_{100-x}$Al$_x$ with $x = 0.7$ and 5. Hereafter these are called 0.7Al and 5Al crystals, respectively. In terms of mass percent, they correspond to Mg-14.0Li-1.0Al, and Mg-13.1Li-7.3Al, respectively. Using the mother ingot, single crystals were grown by the Bridgman method at a growth rate of 2.5 mm/h under argon in a BN crucible. The single crystals were annealed at 450 °C for 72 h for solution treatment. Furthermore, cyclic heat-treatment between 200 and 300 °C (i.e., the temperature was lowered from 300 °C to 200 °C and then it was increased again to 300 °C at the rate of 50 °C/h) was repeated 7 times to remove grown-in dislocations in the single crystal; the effectiveness of this process has previously been reported [14]. For 0.7Al and some 5Al crystals, further

annealing at 450 °C for 5 h followed by ice water quenching (WQ) was conducted to obtain the bcc single-phase microstructure, as described in detail later. Hereafter, this specimen is called 5Al(WQ), and the specimen with only cyclic annealing is called 5Al(w/o WQ). The microstructure and constituent phases in the single crystals were identified by powder X-ray diffraction (XRD) analysis and transmission electron microscopy (TEM).

Rectangular $2.0 \times 2.0 \times 5.0$ mm^3 specimens were cut by electric discharge machining for compression testing. The loading axis orientation was mainly chosen to be $[\bar{1}49]$ where the Schmid factor of the $(\bar{1}01)[111]$ primary slip system had a maximum value of 0.500. Other specimens with three different loading axes of $[\bar{1}\ 4\ 18]$, $[\bar{1}\ 4\ 5.8]$, and $[\bar{1}\ 4\ 4.5]$ on the [410] zone axis were also prepared to examine the orientation dependence of the plastic behavior. The Schmid factors for the expected slip systems at each loading orientation are listed in Supplementary Table 1. Compression tests were conducted at a nominal strain rate of $1.67 \times 10^{-4}\ \text{s}^{-1}$ in vacuum at room temperature (RT). Slip markings introduced in the deformed specimens were observed using an optical microscope (OM).

By the X-ray back Laue analysis, the successful fabrication of single crystals was confirmed in all the crystals. Fig. 1(a–c) and (d–f) show the bright TEM image of the microstructure and the corresponding diffraction pattern (DP) obtained in the single crystals. In addition, Fig. 1

(g) shows the powder XRD profiles of the alloys. In 0.7Al, no precipitate was observed [Fig. 1(a)], and the XRD confirmed that the crystal was mostly composed of the bcc-single-phase, although small peaks derived from the hcp-phase were also observed, probably owing to the loss of Li during preparation. The small dots in the TEM image in Fig. 1(a) may correspond to oxide formed during the fabrication of the TEM sample owing to the high reactivity of Li. The constituent phase was affected by the heat treatments in 5Al. In 5Al(w/o WQ), some precipitates were observed in the bcc-matrix-phase as shown in the inset in Fig. 1 (b); however, the precipitates were diminished by quenching from 450 °C [Fig. 1(c)]. The variation in constituent phase is obvious in the XRD profiles shown in Fig. 1(g). In 5Al(w/o WQ), many additional peaks can be observed along with those from the bcc-matrix phase. Those additional peaks are from AlLi and α-hcp phases. However, those additional peaks vanished in the 5Al(WQ) crystal, which was entirely composed of bcc-single-phase as similarly to the 0.7Al crystal. However, broadening of the foot of the diffraction peaks was observed in 5Al(WQ) for all peaks in Fig. 1(g). Correspondingly, some diffuse extra spots were observed around the bcc fundamental spot in the DP of 5Al(WQ) in Fig. 1(f).

Fig. 2(a) shows the variation in yield stress versus loading orientation for various alloy compositions and heat treatments. To examine the orientation dependence of the plastic deformation behavior, the
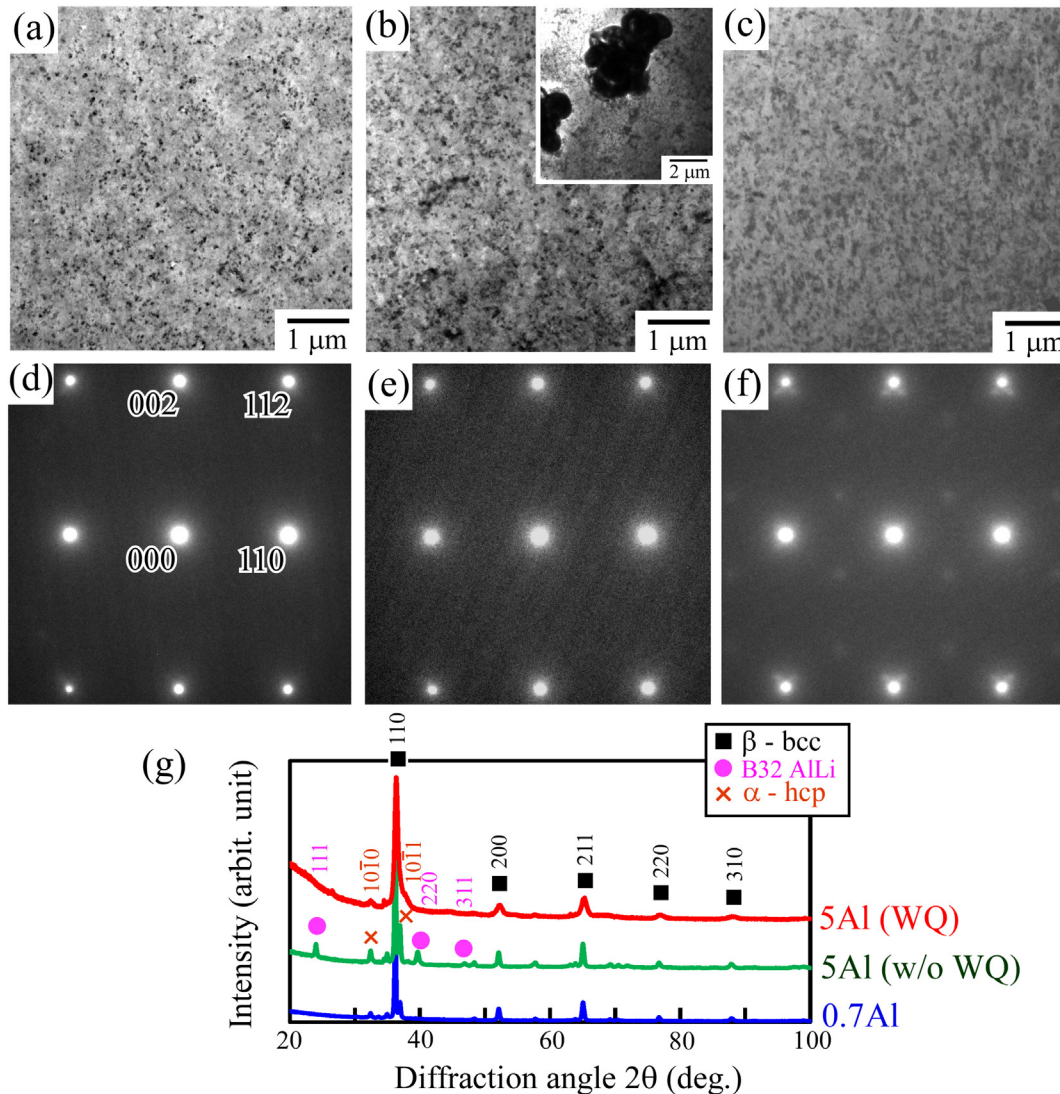

Fig. 1. (a–c) TEM bright-field images of the microstructure observed along $[\bar{1}10]$ in the single crystals; and (d-f) corresponding selected area electron diffraction (SAED) patterns in the (a, d) 0.7Al, (b, e) 5Al(w/o WQ), and (c, f) 5Al(WQ) crystals. (g) Corresponding powder XRD profiles.

tests were conducted at four different loading axes. In bcc-structured crystals, the {101}⟨111⟩ slip is generally reported as an operative deformation mode. Here, the angle "χ" between the expected ($\bar{1}$01) slip plane and the maximum resolved shear stress plane (MRSSP) in the [111] zone is supposed to govern the orientation dependence of the plastic deformation behavior [5,6]. The loading axes selected in this study correspond to χ = −15° at [$\bar{1}$ 4 18], χ = 0° at [$\bar{1}$49], χ = 15° at [$\bar{1}$ 4 5.8], and χ = 25° at [$\bar{1}$ 4 4.5] as shown in Fig. 2(b). In Fig. 2(a) the yield stress of the Mg-35 at.%Li single crystal previously reported by Saka and Taylor [4] is displayed for comparison. The results demonstrate that the yield stress varies with the alloy composition and heat-treatment condition. The addition of 0.7 at.% Al increased the yield stress compared to that of Mg-35Li, but the increase was only ~10 MPa. However, the yield stress was drastically increased by increasing the Al content to 5 at.%; moreover, the increase changed significantly depending on the heat treatment. For 5Al(w/o WQ), the increase in yield stress compared to that in Mg-35Li was ~110 MPa, but it reached ~400 MPa in 5Al(WQ). Furthermore, the crystal orientation dependence of yield stress showed different features in the different alloys. The Mg-35Li crystal showed almost no variation in yield stress with the loading orientation at RT [4], but in 0.7Al the yield stress showed a slight tendency to increase as χ decreased. The tendency of the yield stress to increase with decreasing χ became more significant for the 5Al(WQ) crystal with its increased Al content; however, such orientation dependence of yield stress was not observed in 5Al(w/o WQ). Fig. 2(c) shows typical stress-strain curves deformed at [$\bar{1}$49]. All the crystals could be deformed to ~20% plastic

strain without failure. In the 0.7Al crystal, serrated flow was observed on the stress-strain curve, similar to that observed in Mg-35Li alloy [4]. Saka and Taylor have suggested that the serrated flow might be due to the formation of a Cottrell atmosphere by nitrogen and/or oxygen [4]. Increasing the added Al from 0.7 to 5.0 at.% diminished the serrated flow accompanied by the increase in flow stress. In 5Al(WQ), a slight yield drop was observed, followed by constant flow stress; this behavior differs from the occurrence of weak work-hardening in 0.7Al and 5Al(w/o WQ).

Fig. 3 shows the deformation markings observed in Mg-Li-Al single crystals deformed to ~2% plastic strain. At all the loading orientations, relatively coarse slip traces were introduced. Regarding the morphology of slip traces introduced in 0.7Al alloy deformed at [$\bar{1}$49] shown in Fig. 3 (a, c): The slip traces were straight and the contrast was very weak on the (1$\bar{2}$1) side surface that is parallel to [111] [Fig. 3(a)]. However, the contrast of the slip trace was strong and wavy on the other side surface, as shown in Fig. 3(c). Similar features on the slip trace morphology were observed in all the 0.7Al and 5Al(WQ) crystals. The faint contrast of the slip trace on (1$\bar{2}$1) demonstrates the Burgers vector of the operative dislocation is parallel to [111] as expected [4–6]; while the wavy morphology on the other side surface, which is a typical feature in bcc-materials, suggests the frequent occurrence of cross-slip. Furthermore, as shown in Fig. 3(b–e), the slip plane varied macroscopically with the loading axis in 0.7Al crystals. The macroscopic slip planes were analyzed by a two-face slip analysis at the center of the specimen, and were determined to be nearly parallel to the ($\bar{1}$01) at [$\bar{1}$49] (χ = 0°). However,
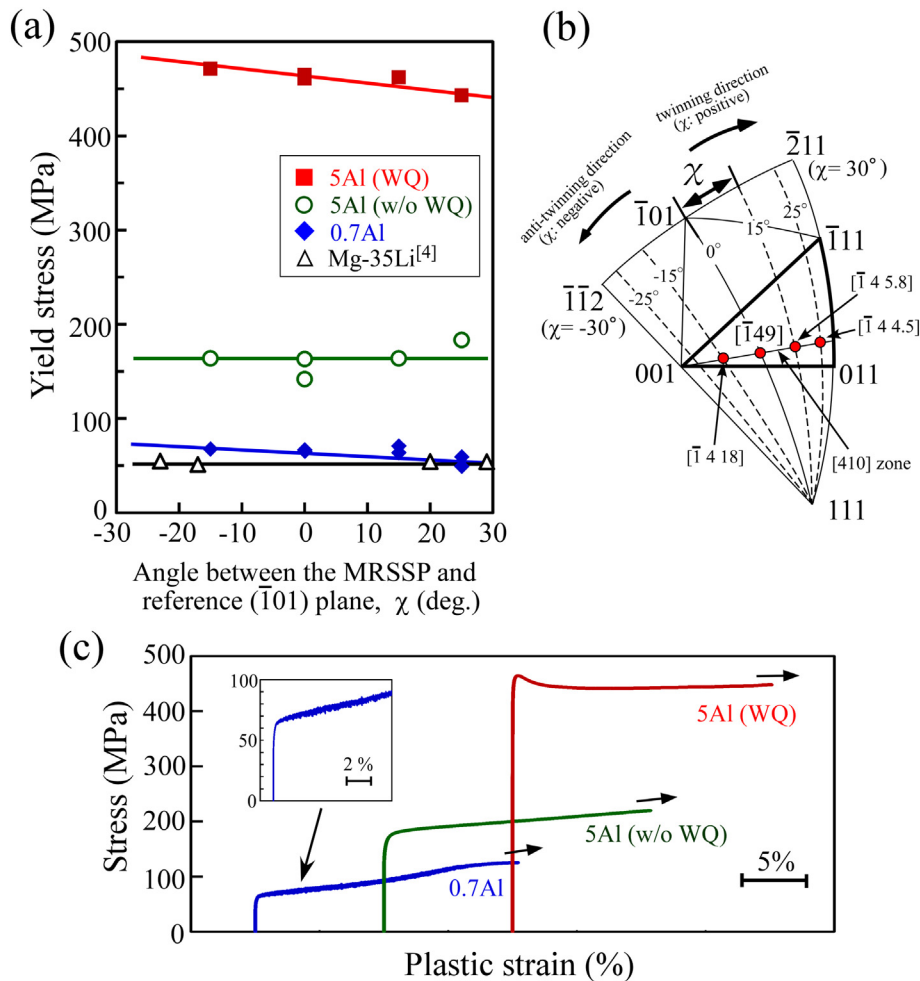

Fig. 2. (a) Variation in yield stress as functions of alloy composition, heat-treatment condition, and loading orientation. The yield stress of a Mg-35 at.%Li single crystal [4] is also plotted for comparison. (b) Stereographic projection of the selected loading axes for the compression tests. (c) Typical stress strain curves deformed at [$\bar{1}$49] loading orientation at room temperature.

the slip plane was deviated from $(\bar{1}01)$ to be $\sim(\bar{8}\ \bar{5}\ 13)$, $(\bar{1}\bar{1}4\ 7)$, and $(\bar{2}11)$ at the $[\bar{1}\ 4\ 18]$, $[\bar{1}\ 4\ 5.8]$, and $[\bar{1}\ 4\ 4.5]$ loading orientations, respectively.

The same analysis was conducted on the 5Al(WQ) crystal as shown in Fig. 3(g–j). The slip plane also varied with loading orientation, but the variation tendency was different from that observed in 0.7Al. Even at $[\bar{1}49]$ ($\chi = 0°$), the slip plane deviated significantly from $(\bar{1}01)$ to $\sim(\bar{4}\ 1\ 3)$. A large difference in the slip plane compared to 0.7Al was also observed at $[\bar{1}\ 4\ 18]$ ($\chi = -15°$). Furthermore, the morphology of the slip traces varied with the heat treatment. Fig. 3(f) shows the deformation markings observed in a 5Al(w/o WQ) crystal deformed at $[\bar{1}49]$; no clear slip trace is observed at any loading orientation. This suggests that the controlling mechanism of the deformation is affected by precipitation in bcc-Mg alloys; a similar feature was previously reported in bcc-Ti alloys [6].

To quantitatively discuss the variations in the slip plane, ψ-χ curve analysis was conducted, and the results are summarized in Fig. 4. The symbol χ represents the angle between the MRSSP in the [111] zone and the reference $(\bar{1}01)$ plane, while ψ is the angle between the observed slip plane and the $(\bar{1}01)$ plane. If the slip plane varies freely depending on the resolved shear stress, it will vary along the dashed line shown in Fig. 4, which corresponds to the MRSSP (i.e., $\psi = \chi$). In Fig. 4, the results previously reported in Mg-35Li [4] are also indicated. In Mg-35Li, the slip plane was almost on the MRSSP at $\chi = 0°$ while it deviated slightly to $(\bar{2}11)$ at $\chi \geq \sim 10°$ and to $(\bar{1}\bar{1}2)$ at $\chi \leq \sim -10°$. An almost identical tendency was observed in the 0.7Al crystal. On the other hand, the deviation of slip traces from MRSSP was significant in the 5Al(WQ) crystal. The slip plane moved significantly toward $(\bar{2}11)$ for a wide range of loading orientations in the region where $-15° \leq \chi \leq 30°$.

As described above, two notable features of the variation in plastic deformation behavior of bcc Mg-Li single crystal by Al addition were found in this study. One is the drastic increase in yield stress in 5Al(WQ) crystals. The significant increase in strength of the Mg-Li alloy by Al-addition was previously reported in some polycrystalline alloys [13,15–17], but it was first confirmed in the single crystal. The yield stress in 5Al(WQ) crystals reached $\sim$440–470 MPa, which is $\sim$8.5 times higher than that in Mg-Li single crystals. This indicates that the apparent critical resolved shear stress (CRSS) for the $\{101\}\langle 111\rangle$ slip reaches to $\sim$220–230 MPa as a rough estimation. The yield stress of conventional Mg-Li alloys is as low as $\sim$100–225 MPa [18] even in the polycrystalline form, which limits the practical applications of Mg-Li alloys. The yield
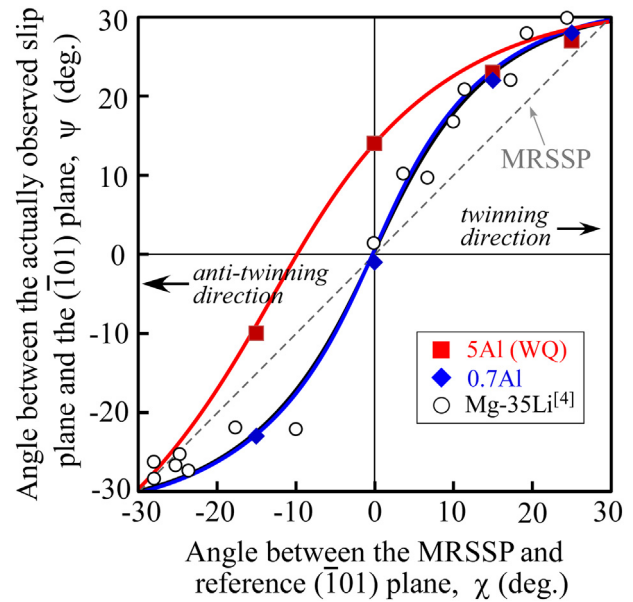

Fig. 4. Variations in the slip plane of [111] dislocations with loading orientation; the so-called ψ-χ curve measured in Mg-Li-Al single crystals compressed at room temperature. The result for a Mg-35Li single crystal [4] is also plotted for comparison.

stress obtained in 5Al(WQ) "single crystals" is unbelievably high, even compared with the values of $\sim$50–350 MPa found in other high-strength hcp Mg-alloys with fine microstructures [19,20]. As the origin of this drastic strengthening, Matsuzawa et al. [15] and Hatta et al. [16] proposed the development of chemical (compositional) modulation in the matrix by spinodal decomposition. Concerning this, Xu et al. conducted an atom probe experiment demonstrating the existence of chemical modulation [17]. Furthermore, Tang et al. recently clarified in the Mg-11Li-3Al-1(Zr, Y) alloy that the chemical modulation is caused by the precipitation of semi-coherent $D0_3$-Mg_3Al nanoparticles [13]. They reported that the drastic strengthening of the alloy is induced by the water-quenching after solution treatment. This is wholly in good agreement with the present result.

Another notable feature is the enhancement of plastic anisotropy by Al-addition. The orientation dependence of the plastic deformation behavior is generally derived from the non-planar three-dimensional
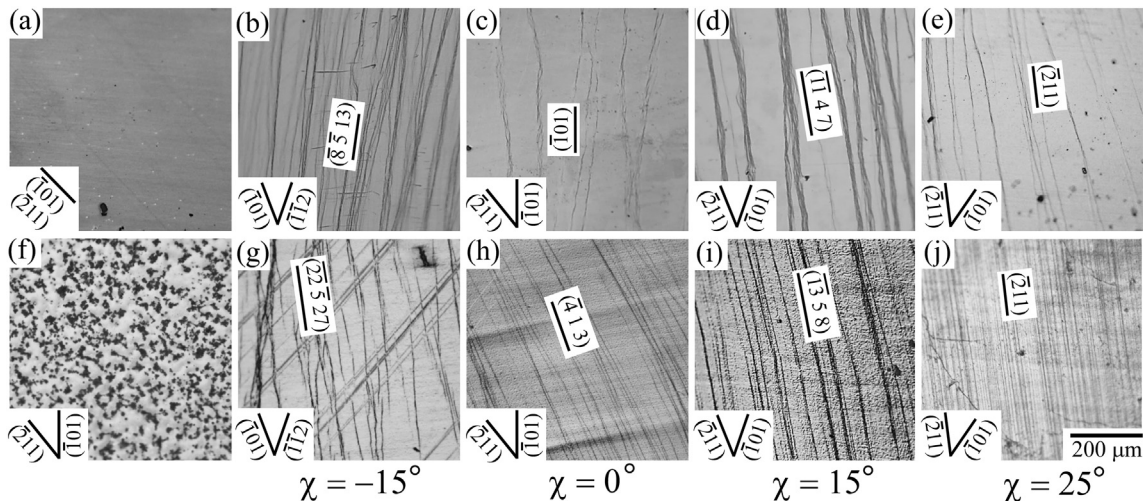

Fig. 3. Variation in deformation markings with loading orientation observed in specimens deformed to $\sim$2% plastic strain. (a–e) 0.7Al, (f) 5Al(w/o WQ), and (g–j) 5Al(WQ). Loading orientation is parallel to (b, g) $[\bar{1}\ 4\ 18]$ ($\chi = -15°$), (c, f, h) $[\bar{1}49]$ ($\chi = 0°$), (d, i) $[\bar{1}\ 4\ 5.8]$ ($\chi = 15°$), and (e, j) $[\bar{1}\ 4\ 4.5]$ ($\chi = 25°$). In the case of Fig. 3(a), the specimen was deformed at $[\bar{1}49]$ and observed on the $(1\bar{2}1)$ side surface, which is parallel to the Burgers vector of the [111] dislocation. Other images taken on other side surfaces that were not parallel to [111].

dislocation core structure of the ⟨111⟩ dislocation in bcc-materials [21]. Our results suggest that the core structure of the ⟨111⟩ dislocation is relatively planar in binary Mg-35Li but changes to a non-planar structure with Al addition at RT. Consequently, the slip plane deviation from MRSSP becomes larger, and the yield stress shows strong orientation dependence in 5Al(WQ); i.e., the compressive yield stress is lower at the loading orientation where the $(\bar{2}11)[111]$ slip is preferentially operative (the twinning sense direction) than where the $(\bar{1}\bar{1}2)[111]$ slip is preferential (the anti-twinning sense direction). Duesbery and Vitek have reported interesting results concerning the variation in the magnitude of plastic anisotropy in bcc-materials [21]. They studied the deformation behavior of various pure bcc metals and found that plastic anisotropy is stronger in group VIB metals (Mo and W) than in group VB metals (Nb and Ta). That is, the increase in valence electron density tends to enhance the plastic anisotropy via the change in dislocation core structure. This agrees with the behavior observed in this study that the plastic anisotropy increased after the addition of Al, which induces an increase in valence-electron to atom (e/a) ratio in alloys; from e/a = 1.65 in Mg-35Li to e/a = 1.70 in 5Al alloy.

Now, the orientation dependences of the elastic properties and the degradation behavior of these alloys in simulated body fluid have been further examined for the development of novel "single-crystalline biodegradable implants". These results will be reported elsewhere.

Supplementary data to this article can be found online at https://doi.org/10.1016/j.scriptamat.2019.07.012.

Declaration of Competing Interest

None.

References

[1] M.K. Kulekci, Int. J. Adv. Manuf. Technol. 39 (2008) 851–865.
[2] M.P. Staiger, A.M. Pietak, J. Huadmai, G. Dias, Biomaterials 27 (2006) 1728–1734.
[3] G.J. Shen, B.J. Duggan, Metall. Mater. Trans. A 38A (2007) 2593–2601.
[4] H. Saka, G. Taylor, Philos. Mag. 43 (1981) 1377–1392.
[5] S.-H. Lee, K. Hagihara, T. Nakano, Metall. Mater. Trans. A 43A (2012) 1588–1597.
[6] K. Hagihara, T. Nakano, H. Maki, Y. Umakoshi, M. Niinomi, Sci. Rep. 6 (2016) srep29779.
[7] M. Tane, S. Akita, T. Nakano, K. Hagihara, Y. Umakoshi, M. Niinomi, H. Nakajima, Acta Mater. 56 (2008) 2856–2863.
[8] J.-Y. Rho, T.Y. Tsui, G.M. Pharr, Biomater. 18 (1997) 1325–1330.
[9] W.A. Counts, M. Friák, D. Raabe, J. Neugebauer, Acta Mater. 57 (2009) 69–76.
[10] K. Hagihara, M. Okubo, M. Yamasaki, T. Nakano, Corros. Sci. 10 (2016) 68–85.
[11] D. Cao, L. Wu, Y. Sun, G. Wang, Y. Lv, J. Power Sources 177 (2008) 624–630.
[12] A. Sanschagrin, R. Tremblay, R. Angers, D. Dubé, Mater. Sci. Eng. A 220 (1996) 69–77.
[13] S. Tang, T. Xin, W. Xu, D. Miskovic, G. Sha, Z. Quadir, S. Ringer, K. Nomoto, N. Bribilis, M. Ferry, Nature Comm 10 (2019) no.1003.
[14] S. Kitajima, M. Ohta, H. Kaieda, J. Japan Inst. Metal. 32 (1968) 164–169 (in japanese).
[15] K. Matsuzawa, T. Koshihara, S. Ochiai, Y. Kojima, J. Japan Inst, Light Met. 40 (1990) 659–665 (in Japanese).
[16] H. Hatta, R. Chandran, S. Kamado, Y. Kojima, J. Japan Inst, Light Met. 47 (1997) 195–201 (in Japanese).
[17] W. Xu, N. Bribilis, G. Sha, Y. Wang, J.E. Daniels, Y. Xiao, M. Ferry, Nat. Mater. 14 (2015) 1229–1236.
[18] G.H. Park, J.T. Kim, H.J. Park, Y.S. Kim, H.J. Jeong, N. Lee, Y. Seo, J.-Y. Suh, H.-T. Son, W.-M. Wang, J.M. Park, K.B. Kim, J. Alloys Compd. 680 (2016) 116–120.
[19] K. Hagihara, A. Kinoshita, Y. Sugino, M. Yamasaki, Y. Kawamura, H.Y. Yasuda, Y. Umakoshi, Acta Mater. 58 (2010) 6282–6293.
[20] M. Okayasu, S. Takeuchi, M. Matsushita, N. Tada, M. Yamasaki, Y. Kawamura, Mater. Sci. Eng. A 652 (2016) 14–29.
[21] M.S. Duesbery, V. Vitek, Acta Mater. 46 (1998) 1481–1492.